



Research papers

## Relative effect of anthropogenic warming and natural climate variability to changes in Compound drought and heatwaves



Sourav Mukherjee <sup>a,\*</sup>, Ashok Kumar Mishra <sup>a</sup>, Moetasim Ashfaq <sup>b</sup>, Shih-Chieh Kao <sup>b</sup>

<sup>a</sup> Glenn Department of Civil Engineering, Clemson University, SC, USA

<sup>b</sup> Oak Ridge National Laboratory, Oak Ridge, TN, USA

### ARTICLE INFO

**Keywords:**

Compound drought and heatwave  
Natural climate variability  
Climate Change  
Global Warming  
Hydroclimatic Extreme Events

### ABSTRACT

Compound drought and heatwave (CDHW) events can be influenced by large scale teleconnections and anthropogenic warming, leading to severe socio-economic impacts across various climate regions. In this study, the relative influence of six different teleconnection patterns and anthropogenic global warming on the global CDHW occurrences is quantified systematically using the instrumental data period, 1982–2016. The results from the study suggest a substantial increase in the CDHW events (1–5 events per year) across various parts of the globe at the beginning of 21st century (2000–2016). A Bayesian approach is implemented to identify the most vulnerable climate regions based on the degree of susceptibility of heatwaves (DSHW) towards drought. As such, top ten most vulnerable regions are selected based on the DSHW magnitude, and a partial correlation analysis is performed to select the natural and anthropogenic drivers of CDHW in those regions, separately. A logistic regression model is then used to determine significant changes in the odds of CDHW due to changes in the selected drivers that suggest a significantly positive, and multiplicative effect of anthropogenic global warming in the top ten most vulnerable climate regions. Finally, the same logistic regression model, integrated with an analytical framework, is applied to determine the relative influence of anthropogenic global warming on the changes in odds of CDHW for the future, 1.5 °C and 2 °C warming limits. The results suggest that relative to the 2 °C global warming, constraining to the 1.5 °C global warming limit may conduce about 17-fold reduction in the odds of CDHW in the most vulnerable climate region, East Asia, 5–8-fold reduction in Western North America, Northern Australia, Central North America, Central Europe, South Asia, and the Mediterranean region, and 3–4-fold reduction in Northeastern Brazil, Eastern North America, and West Asia.

### 1. Introduction

Compound drought and heatwave (CDHW) events have had multiple societal and eco-hydrological impacts including loss of crop yield (Ciais et al., 2005; Zampieri et al., 2017), increased wildfires and tree mortality (Allen et al., 2010), and health hazards (Poumadère et al., 2005). CDHW events are typically triggered by anticyclonic flow patterns (Trenberth and Fasullo, 2012), followed by land–atmosphere feedback processes that modulate the surface energy budget (Mukherjee et al., 2020; Mukherjee and Mishra, 2020). Natural modes of climate variability are instrumental in influencing global circulation patterns that lead to conditions favoring the development of anticyclonic regimes over terrestrial regions (Mukherjee et al., 2020; Pepler et al., 2019). Observations indicate a poleward expansion of these regimes in both hemispheres during the past few decades, which is attributed to intensification and

poleward shift in main storm tracks in mid-latitudes, associated with warming (Lu et al., 2007; Pepler et al., 2019; Trenberth et al., 2014; Yin, 2005).

The anticyclonic anomalies in the atmosphere are accompanied with clear skies or lack of moisture in the lower atmosphere making conditions less conducive for precipitation and thereby facilitating drought conditions. The lack of surface moisture leads to excessive sensible heating at the expense of decreased latent energy or evapotranspiration, causing surface warming. The prolonged period of high surface temperatures eventually lead to heatwaves (HW) (Horton et al., 2016; Stéfanon et al., 2014), resulting in the occurrence of CDHW events. Additionally, the rise in surface air temperature further exacerbates drought conditions by initiating a land–atmosphere feedback loop with the soil moisture by increasing the atmospheric demand (leading to increased evapotranspiration). This feedback process is very common in

\* Corresponding author.

E-mail address: [souravm@g.clemson.edu](mailto:souravm@g.clemson.edu) (S. Mukherjee).

the anticyclonic weather regimes and is generally referred as the soil-temperature coupling (Betts et al., 1996; Seneviratne et al., 2010; Whan et al., 2015). Anthropogenic climate change has already accelerated such processes leading to increased frequency of CDHW events across many parts of the globe (Mazdiyasni and AghaKouchak, 2015; Mukherjee and Mishra, 2020; Sun et al., 2017, 2018; Zhang et al., 2019b).

Given the role of temperature anomalies in the occurrence of CHDW events, drought quantification using only precipitation may lead to underestimation of drying (Dai and Zhao, 2017), which can lead to uncertainties in the characterization of CDHW events (Mukherjee et al., 2020; Mukherjee and Mishra, 2020). Therefore, it is imperative that soil moisture, and surface temperature anomalies are incorporated in the estimation of CDHW using the energy budget framework. To this end, Palmer Drought Severity Index (PDSI; Wells et al., 2004) is a comprehensive drought index that incorporates hydroclimatic variables relevant to the estimation of drought under the changing climate (Mukherjee et al., 2018). Furthermore, as previously noted, the large scale natural modes of climate variability are instrumental in the formation of anticyclonic regimes and that anthropogenic footprint is detectable in the intensification of conditions that are conducive for the occurrence of extreme dry and hot conditions (Hassan and Nayak, 2020; Lau and Kim, 2012; Pepler et al., 2019). Therefore, there is a need to establish analytical frameworks that not only identify relevant modes of climate variability, that exert influence on distribution of CHDW events across the globe, but also incorporate the relative influence of anthropogenic warming (ANT) on the evolution of CDHW events (Hao et al., 2018, 2019; Zhang et al., 2019b).

In this study, we present a comprehensive global analysis on the relative effect of anthropogenic warming and natural climate variability on CDHW events, for the first time. First, we focus on the identification of natural and anthropogenic climate forcings that play a significant role in the occurrence of CDHW events during the 1982–2016 historical period. Subsequently, we estimate the possible increase of such events at 1.5 °C and 2 °C future warming scenarios and discuss its implication for mitigation strategies. The rest of the manuscript is structured as follows: Section 2 focuses on the data and methodology applied in the study; the results and relevant discussions are provided in Section 3; and finally, the summary of major findings and concluding remarks are provided in Section 4.

## 2. Data and methodology

### 2.1. Data

We selected 26 climate regions across the globe, proposed under the IPCC-AR5, as the study area (as shown in Fig. S1). Gridded daily global maximum and minimum 2 m air temperature (Tmax and Tmin) at 0.5° spatial resolution was obtained from the Climate Prediction Center (CPC) (from CPC Global Temperature data provided by the NOAA/OAR/ESRL PSD, Boulder, Colorado, USA, from their website at <https://psl.noaa.gov/data/gridded/data.cpc.globaltemp.html>). Gridded daily global precipitation (Pr) at 1° spatial resolution was obtained from the Global Precipitation Climatology Center (GPCC; Schamm et al., 2015). Available water content (AWC) was obtained from the global texture derived AWC dataset by Webb et al. (2000). All datasets were regridded to the same 2.5° spatial grids for the calculation of global weekly CDHW events from 1982 to 2016.

To evaluate the relative influence of anthropogenic warming and natural climate variability of the CDHW events, we calculated global mean temperature changes, and selected six different natural modes of climate variability for analysis (Table S1). For the calculation of global mean temperature changes, global gridded monthly temperature anomaly data provided by HadCRUT4 (Morice et al., 2012) was obtained from <https://crudata.uea.ac.uk/cru/data/temperature/>. We further re-calculated the anomalies over the globe using the pre-

industrial era (1861–1890) as the baseline period, and then obtained the global mean temperature change (referred hereafter as “ANT” in this study). The six natural modes of variability include Southern Oscillation Index (SOI), Dipole Mode Index (DMI/IOD), Southern Annular Mode (SAM), Arctic Oscillation (AO), North Atlantic Oscillation (NAO), and Pacific Decadal Oscillation (PDO). The SOI is available from the Bureau of Meteorology (<http://www.bom.gov.au/climate/current/soihtm1.shtml>), and IOD was obtained from the NOAA Climate Prediction Centre (NOAA CPC; <http://www.cpc.ncep.noaa.gov/>). The monthly values of SAM, AO, NAO, and PDO were also retrieved from NOAA CPC.

To assess the impacts of warming, we first used a 21-year window (2008–2028) centered on year 2018 to calculate the current day warming (hereafter referred to as the current world). The warming level in the current world is estimated based on the globally averaged monthly temperature outputs from 35 Coupled Model Intercomparison Project Phase-5 (CMIP5; <https://esgf-node.llnl.gov/search/cmip5/>) Global Climate Models (GCMs; Table S2) under the Representative Concentration Pathways 8.5 (RCP8.5) emission scenario. We chose the RCP8.5 scenario, as it matches the observed emissions more closely (Sanford et al., 2014) compared to the other RCPs (RCP2.6, RCP4.5, and RCP6).

### 2.2. Estimation of Compound drought and heatwave (CDHW) events

CDHW events are estimated following the procedure proposed in Mukherjee et al. (2020). Drought estimation at weekly time scale can help to retain the memory of soil temperature and moisture inherited within a short time-scale (Mukherjee et al., 2020). This approach not only captures the diurnal feedback loop but also produces a considerable sample size required in the statistical analysis of rare events such as the co-occurrence of HW and drought. In this study, we define a CDHW event as a HW event that occurred during the drought weeks over a given location and temporal period.

A threshold-based approach was used to identify CDHW events during 1982–2016. At each grid point, the 10th percentile of weekly self-calibrated PDSI (wPDSI\_sc) for the reference period, 1982–2011 were obtained as a threshold, and any wPDSI\_sc value below that threshold was estimated as a drought week for the period, 1982–2016 (Mukherjee et al., 2020; Mukherjee and Mishra, 2020). CDHW events were then identified when daily Tmax value exceeded the 90th percentile (TX90pct) (Fischer and Knutti, 2015; Meehl and Tebaldi, 2004; Perkins et al., 2012; Unkašević and Tošić, 2013) for 3 or more consecutive days during these drought weeks. The TX90pct was calculated for each calendar day as the 90th percentile of daily Tmax over each 31-day window during the 30 years (1982–2011) climatological period (Fischer and Schär, 2010).

### 2.3. Measurement of degree of susceptibility of HW (DSHW) towards drought

To get a measure to which it is more likely that HW and drought will co-occur in a particular location, we estimated the degree of susceptibility of HW towards drought (DSHW) in the historical period. The DSHW was estimated by using a Bayesian approach, based on the conditional formulation of CDHW events followed by a statistical test for significance. First, probability ( $pe$ , and  $pc$ ) of occurrence of two mutually exclusive extreme events, HW events with and without an already existing drought (that influences the background state of the climate) were estimated based on the observational record across the globe. Statistically significant (at 5% significance level)  $pe/pc$  ratio greater than 1 was obtained using the two-proportion z-test (or Chi-square test). The z-statistic is based on a standard normal distribution. Therefore, to remove the normality assumption, the results were obtained for the two mutually exclusive events (i.e., HW events with and without an already existing drought) by resampling, producing 1000 realizations each with replacement. The resampling is performed based on the following steps:

- a. First the number of days with drought occurrences ( $=d$ ), no drought occurrences ( $=nd$ ), HW occurrences ( $=h$ ), and non-occurrences ( $=nh$ ), are recorded for a given grid point.
- b. The pe and pc values from the above information is used to calculate the z-statistics from the observed sample.
- c. A matrix consisting of binary elements (1 and 0), is generated based on the number of HW occurrences ( $h$ ) indicated by the number of “1”s and non-occurrences ( $nh$ ) indicated by the number of “0”s.
- d. For a given realization (out of total 1000 selected here), total  $d$  samples are chosen with replacement from the binary matrix and stored as  $M1$ . Subsequently, pe is calculated as the sum of all 1 s and zeroes from the matrix,  $M1$ , divided by the number of drought days ( $d$ ).
- e. Similarly, total  $nd$  samples were chosen with replacement from the binary matrix and stored as  $M2$ . Subsequently, pc is calculated as the sum of all 1 s and zeroes from the matrix,  $M2$ , divided by the number of non-drought days ( $nd$ ).
- f. The z-statistics from the sampling distribution is calculated based on the pe and pc values from the sampling distribution.
- g. Finally, 1000 samples of the z-statistics for the sampling distribution are generated by repeating the steps in (c, d, e, and f) 1000 times.

Finally, the proportion of the z-statistic from the sampling distribution which had absolute values as large or larger than that observed z-statistic is calculated. We rejected the null hypothesis of equal proportions if that proportion was greater than 0.05. The  $pe/pc$  ratio showing a significantly greater than 1 value was thus obtained at each grid point and defined as the DSHW in this study. The detailed formulation of z-statistics and the DSHW is provided in Appendix A of the

$$\text{logit}(Y) = \ln\left(\frac{\pi}{1-\pi}\right) = \underbrace{(\beta_1 X_1 + \beta_2 X_2 + \dots + \beta_n X_n)}_{\text{Natural Component}} + \underbrace{\beta_{\text{ANT}} X_{\text{ANT}}}_{\substack{\text{Anthropogenic} \\ \text{Component}}} + \alpha, \quad (2)$$

supplemental information.

#### 2.4. Estimation of partial correlation

Partial correlation is the measure of association between two variables, while controlling or adjusting the effect of one or more additional or confounding variables. The effect of the confounding variables is adjusted based on their weights calculated as their regression coefficients. Partial correlation technique has been employed to derive inferential impact of multiple large scale teleconnection patterns (e.g., ENSO, PDO, NAO, and IOD) on temperature extremes and drought across many regions of the globe (Ashok and Saji, 2007; Hu and Huang, 2009; Manatsa et al., 2008; Mukherjee and Mishra, 2020; Rajagopalan et al., 2000; Zhang et al., 2019a). In this study, a non-parametric spearman's rank correlation analysis was performed to identify possible drivers (Large-scale oscillation patterns and ANT) that influence the CDHW events. Hence, statistically significant (at 5% significance level) Spearman's partial correlation between the region-wise area weighted number of MT-CDHW days and the interannual variability of the large-scale climate indices and ANT for the period, 1982–2016 were estimated for the selected climate regions, such that,

$$r_{xyz} = \frac{r_{xy} - r_{xz}r_{yz}}{\sqrt{(1 - r_{xz}^2)(1 - r_{yz}^2)}} \quad (1)$$

where  $r_{xyz}$  is the relative correlation between  $\times$  (area weighted number of MT-CDHW days), and  $y$  (large scale climate indices, or ANT) with the effect of  $z$ , either of the other indices (or ANT) are removed. In order to

account for the inter-dependence of different climate modes (Meyers et al., 2007; Perkins et al., 2015) and ANT, we employ partial correlation technique (equation 8) to isolate the influence of individual forcing.

#### 2.5. Measurement of odds of occurrence of CDHW events

Previous studies have confirmed the link between the odds of occurrence of extreme events and other climate variables using logistic regression (Mahlstein et al., 2012; Zhai et al., 2005). In this study, we investigated the relative effect of large-scale teleconnection patterns and anthropogenic warming based on odds ratios calculated using the Firth logistic regression model. The odds of occurrence of CDHW events in any month is calculated using the interannual variability of large-scale climate indices and changes in the global mean temperature during the period, 1982–2016 as predictors. A detailed discussion on the application of the logistic regression model is discussed in the following section.

##### 2.5.1. Logistic regression model

We applied a multiple-predictor based Firth logistic regression model that is a special form of generalized linear model (Lindsey, 2000) to estimate the penalized regression coefficients corresponding to natural and anthropogenic variability of the climate. The Firth's model applies penalized likelihood estimation rather than performing the conventional maximum likelihood estimation to obtain the penalized regression coefficients. The penalization allows for convergence of the likelihood to finite estimates in conditions of separation and also with sparse data and therefore, may alleviate overfitting (Albert and Anderson, 1984).

In our analysis, we used the following logistic regression model:

where  $\left(\frac{\pi}{1-\pi}\right)$  is the odds of having more than two CDHW events per year;  $X_1, X_2, \dots, X_n$  are the large scale climate indices used in the model and  $X_{\text{ANT}}$  is the change in global mean temperature with respect to the pre-industrial period, 1861–1900;  $\alpha, \beta_1, \beta_2, \dots, \beta_n$ , and  $\beta_{\text{ANT}}$  are the corresponding penalized regression coefficients (or scaling factors). Once the model was fitted for the observational distribution the penalized regression coefficients were obtained that we refer as the scaling factors in this study.

#### 2.6. Estimating odd ratio for 1.5 °C, and 2 °C global warming

One of our objectives is to answer the science question – “How much more likely will there be a CDHW day (in a month) at 1.5 °C and 2 °C global warming scenarios than there is at the current level of anthropogenic warming?”. This was achieved by changing the anthropogenic component to different warming levels (Current, 1.5 °C, and 2 °C), while keeping the natural component constant in the regression model. We estimated the current level of warming based on the average of monthly temperature anomalies (estimated with respect to the pre-industrial period, 1861–1890) for the current world. Finally, the odd ratio (OR) of monthly occurrence CDHW day for the future warming limits (1.5 °C, and 2 °C) to that for the current warming level was estimated as,

$$\begin{aligned}
OR_{T^{\circ}C} &= \frac{\left(\frac{\pi}{1-\pi}\right) T^{\circ}C}{\left(\frac{\pi}{1-\pi}\right) Current} \\
&= \frac{\exp\left(\alpha + \underbrace{(\beta_1 X_1 + \beta_2 X_2 + \dots + \beta_n X_n)}_{\text{Natural Component}} + (\beta_{ANT} T)\right)}{\exp\left(\alpha + \underbrace{(\beta_1 X_1 + \beta_2 X_2 + \dots + \beta_n X_n)}_{\text{Natural Component}} + (\beta_{ANT} X_{Current})\right)} \\
&= \frac{\exp(\beta_{ANT} T)}{\exp(\beta_{ANT} X_{Current})} \quad (3)
\end{aligned}$$

where  $T$  is the selected warming limit of 1.5 °C, and 2 °C, and  $X_{Current}$  refers to the current warming level with respect to the pre-industrial period.

### 3. Results

#### 3.1. Annual increase in the number of CDHW events

The number of CDHW events has increased annually during the 21st century (Post-2000) compared to that observed during the last two decades of the 20th century (Pre-2000) (Fig. 1a). Figs. S2a and 1(a) show the spatial distribution of the average number of events during the Pre-2000 and Post-2000 periods, and the corresponding difference in the same between the two periods, respectively. Fig. 1(b) show the nonparametric probability density for the average number of CDHW events during the Pre-, and Post-2000 periods of the globe. We also performed the Kolmogorov-Smirnov and Wilcoxon rank sum tests to show that there is a statistically significant (at 5% significance level) difference between the distributions and medians of the CDHW events,

respectively, between these two periods. Our analysis suggests an overall annual range of 1–5 events during the Post-2000 period (Fig. S2b) with major portions included in most of the climate regions showing an increase of 1–3 number of events per year (Fig. 1a). Those regions include the Southern parts of WNA and CAN, Eastern NAU, eastern and southeastern SAF, northeastern SAS, eastern ENA, northern MED, central NEU, and almost all over WAS, CEU and NEB. In addition to that, regions such as the southern EAS, eastern ALA, western CGI, and central AMZ show an increase of as high as 5 annual events during the Post-2000 period. However, CGI and ALA are excluded from rest of the analyses due to poor quality of available data over these regions.

#### 3.2. Degree of susceptibility of HW (DSHW) towards drought

We focus on finding the locations where it is significantly more likely to have HW and drought co-occurred on a particular day based on observations (Fig. S3). We find that majority of grid points show higher DSHW towards a persistent drought week ( $pe/pc$  greater than 1; Fig. 1c). However, the percentage of total area showing such DSHW varies across the different climate regions (Fig. 1d). Climate regions, SEA, WAF, EAF, CAM, NAS, TIB, and CGI exhibit more than half of the area with statistically significant  $pe/pc$  ratio greater than 1, while SAH, WSA, SSA, and AMZ have less than half of the total area satisfying such conditions. More importantly, the rest of the 26 climate regions, CAN, CEU, EAS, WNA, WAS, NEB, ENA, NAU, SAS, MED, CAS, ALA, NEU, SAF, and SAU exhibit more than 2/3rd of the area that shows statistically significant degree of susceptibility of HW under an ongoing drought condition with majority of them showing  $pe/pc$  ratio as high as more than 5 (Fig. 1c). Therefore, out of all 26 climate regions considered in this study, we selected the top 10 climate regions that show a significant DSHW over more than 2/3rd of the total area (Fig. 1d). Interestingly, these regions also show an

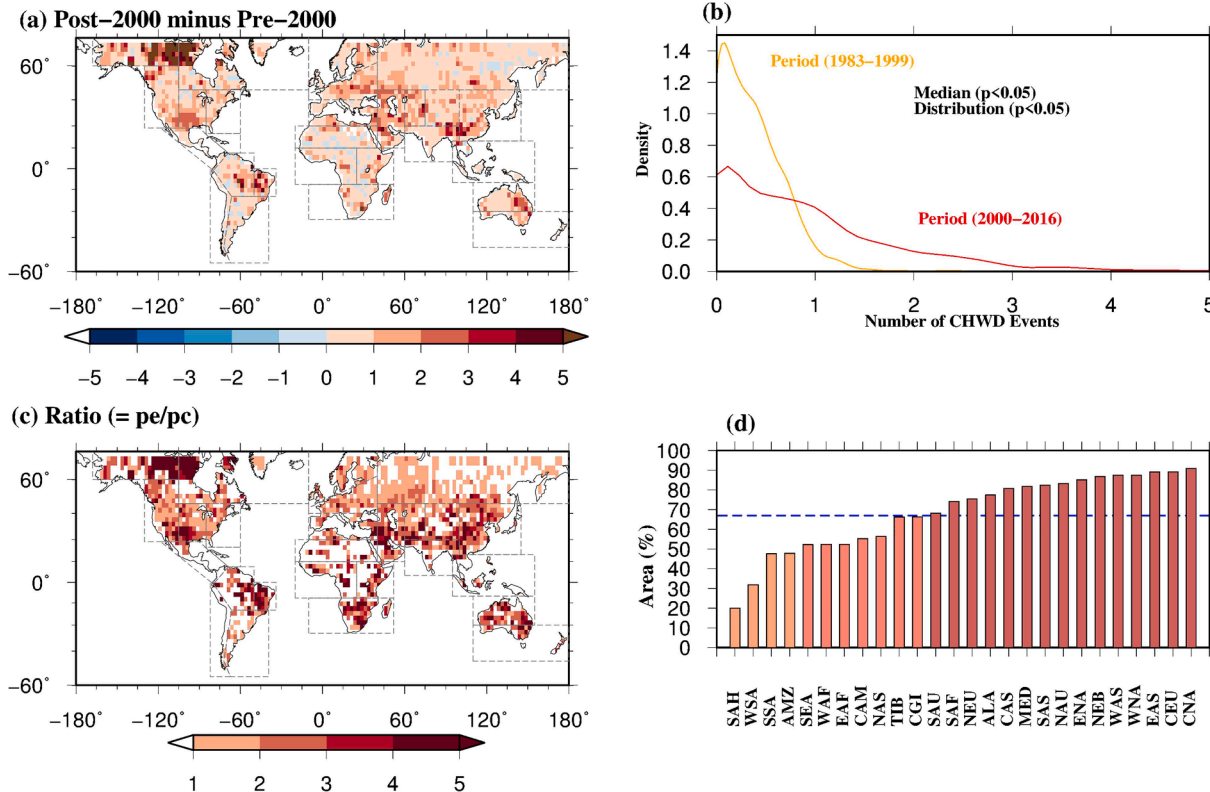


**Fig. 1.** (a) Difference between the average number of CDHW events during the Pre-2000 period (1983–1999) and Post-2000 period (2000–2016), (b) kernel density plot of the average number of CDHW events during the two periods of the globe, (c) spatial distribution of the ratio of the probabilities where the probability of heat wave day conditioned on drought (pe) is significantly (at 5% significance level) greater than the probability of heat wave day conditioned on no drought (pc), and (d) percentage area of each climate region showing significantly (at 95% confidence level) greater probability of heat wave day conditioned on drought (pe) than that conditioned on no drought (pc).

increase in the number of CDHW events during the Post-2000 period, as shown in Fig. 1a. Consequently, we performed the rest of the analyses based on these 10 climate regions.

### 3.3. Possible natural and anthropogenic drivers

Previous studies suggest possible links between the large-scale global circulation patterns or oceanic variabilities and anticyclonic regimes in both the Northern and Southern Hemisphere (Abid et al., 2020; García-Serrano et al., 2017; Pepler et al., 2019; Singh et al., 2021; Song and Zhou, 2013; Wang and Zhang, 2002). Therefore, understanding and exploring such a relationship is key to identify the attributable factors behind the occurrence of compound events such as the CDHW for the climate regions that exhibit significant DSHW towards drought over more than 2/3rd of the total area. More precisely, we explore possible links between the monthly total number of CDHW (MT-CDHW) days and the interannual variability in the natural climate (Song and Zhou, 2013) as well as the influence of rise in ANT on such extremes during the historical period.

We selected six (Table S1) natural modes of climate variability that exert major influence on the variability of climate globally at seasonal to decadal time scale. To represent the interannual variability of these modes, monthly anomalies of their representative indices and global mean temperature were smoothed by applying a 12-month running mean filter. Since areal extent varies across different regions, area weighted MT-CDHW days were estimated for all selected climate regions. Fig. 2a show only the statistically significant (at 5% significance level) Spearman's partial correlation (see Methods) between the region-wise area weighted MT-CDHW days and the interannual variability of the large-scale climate indices and ANT for the period, 1982–2016 for the selected climate regions.

The results suggest that ANT exerts strong influence on the observed MT-CDHW days during the period 1982–2016 (Fig. 2a), which is consistent with previous studies that have suggested a progressive global warming footprint in the occurrence of heatwaves (Deng et al., 2018), droughts (Wang et al., 2016), and CDHW events (AghaKouchak et al., 2014) at the regional scale.

In addition to that, several natural modes of climate variability also show a significant but relatively weak correlations with the occurrences of CDHW events during the analyses period.

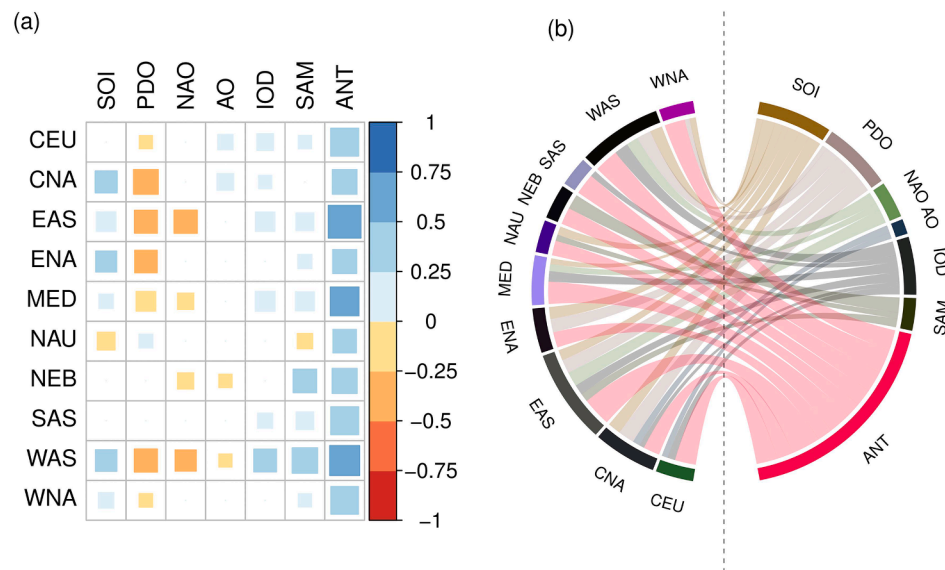


**Fig. 2.** (a) Correlogram showing the significant (at 5% significance level) partial correlation between the number of monthly CDHW days and the interannual variability of large-scale climate indices during the 1982–2016 period based on non-parametric Spearman's rho, and (b) Chord diagram showing the large-scale indices chosen based on the mechanistic explanation.

#### 3.3.1. Southern oscillation index

Interannual variability of SOI show statistically significant positive correlation with the area weighted MT-CDHW days for the regions CNA (0.3), EAS (0.273), ENA (0.27), MED (0.13), WAS (0.29) and WNA (0.15), and negative correlation for the NAU (−0.2) (Fig. 2a). It is well known that ENSO is one of the major natural modes of climate variability that exerts substantial influence in the global occurrences of simultaneous droughts (Singh et al., 2021). It tele-connects with remote regions through Rossby wave trains that either originate directly from central equatorial Pacific or propagate as a result of inter-basin interactions (Abid et al., 2020; Wang et al., 2017).

#### 3.3.2. Indian ocean dipole

IOD show significant positive correlation for the climate regions such as CEU (0.17), CNA (0.1), EAS (0.23), MED (0.24), SAS (0.14), and WAS (0.32) (Fig. 2a). The role of IOD has been suggested in the formation of anticyclonic circulation over the Eastern Asia leading to unusual summer temperature in 1961 and 1994 (Saji and Yamagata, 2003). The IOD-induced divergent flow and diabatic heating anomalies excite the Rossby wave train propagation during summer towards the EAS climate region (Qiu et al., 2014). Impact of IOD is also linked to the circulation changes over the Europe and North America (Guan and Yamagata, 2003; Saji and Yamagata, 2003), and negative rainfall anomaly over the WAS climate region (Barlow et al., 2002). A significant warming trend and a 10–20% reduction in rainfall is reported over the Indian subcontinent (included in the SAS climate region) over 1901–2012 due to rapid warming of the Indian Ocean (positive IOD phase) (Roxy et al., 2015).

#### 3.3.3. North atlantic oscillation (NAO)

Strong influence of NAO over European heat wave and drought is evidenced through observational studies that suggest excitation of stationary wave train that facilitates anticyclonic weather regimes over the region (Cassou et al., 2005). Moreover, NAO can be associated with the North Atlantic Jet variability that has strong influence over temperature and precipitation variability over the US and Europe (Mahlstein et al., 2012; Trouet et al., 2018). This is also evident in our correlation analysis that show statistically significant Spearman's correlation coefficient over MED (−0.16) (Fig. 2a). Besides MED, three more climate regions (EAS (−0.33), NEB (−0.16), and WAS (−0.28)) also show a significant correlation with the MT-CDHW days (Fig. 2a). Except for NEB, where

the Atlantic Multidecadal Oscillation (AMO) is the major driver (Knight et al., 2006), the NAO show marked influence on the precipitation and temperature variability over WAS (Filippi et al., 2014) and EAS (Bollasina and Messori, 2018). Note that due to the short span of the temporal period 1982–2016, we did not include AMO in our analysis.

### 3.3.4. Pacific decadal Oscillation (PDO)

PDO show relatively strong negative correlation for three north American regions: CNA ( $-0.38$ ), ENA ( $-0.31$ ), and WNA ( $-0.11$ ) (Fig. 2a), which is consistent with the findings of previous studies that have documented significant influence of PDO on drought and heat wave events across the conterminous US (Dulière et al., 2013; McCabe et al., 2004; Peterson et al., 2013). Moreover, we find negative correlation with the interannual variability of PDO (Fig. 2a) and the number of MT-CDHW days over the EAS ( $-0.33$ ), and WAS ( $-0.33$ ) (Fig. 2a) climate regions, which is also supported by previous observational studies (Yu et al., 2018). However, significant correlations between variability in PDO and climate regions such as NAU ( $0.11$ ), CEU ( $-0.11$ ), and MED ( $-0.24$ ) indicate a possible indirect influence on the CDHW events over these regions. Therefore, we exclude such influences in the further analysis of CDHW events over these regions.

### 3.3.5. Arctic Oscillation (AO) and Southern Annular mode (SAM)

SAM shows positive correlation for the climate regions in the northern hemisphere such as, CEU ( $0.11$ ), EAS ( $0.2$ ), ENA ( $0.12$ ), MED ( $0.22$ ), SAS ( $0.19$ ), WAS ( $0.4$ ), and WNA ( $0.1$ ) (Fig. 2a). On the other hand, significant correlation is found for climate regions, NAU ( $-0.14$ ), and NEB ( $0.34$ ) in the southern hemisphere (Fig. 2a). It is evidenced that positive SAM has a strong influence on the frequency and poleward expansion of anticyclones in the southern hemisphere (Gillett et al., 2006; Marshall et al., 2014; Pepler et al., 2019) with intensification of Rossby wave in the eastern Australia. However, except for EAS (Wu et al., 2015), there is no such evidence of SAM index in the northern hemisphere therefore the impact of SAM is not considered in the further analysis of CDHW events over the northern hemisphere climate regions (CEU, ENA, MED, SAS, WAS, and WNA). On the other hand, AO that has significant influence over the increased frequency and expansion of anticyclones in the northern hemisphere (Pepler et al., 2019) also show significantly weak correlation for climate regions, CEU ( $0.14$ ), CNA ( $0.17$ ), NEB ( $0.19$ ), and WAS ( $0.1$ ). In our further analysis, we exclude the effect of AO over the climate regions such as WAS, and NEB.

Finally, based on the correlative evidence provided in this section, a chord diagram is presented (Fig. 2b) to show the selected large-scale climate indices along with the ANT that has a significant impact on the occurrence of CDHW events for the selected climate regions.

### 3.4. Scaling factors associated with CDHWs

The selected large-scale meteorological perturbations, and ANT (Fig. 2b) were used as independent variables to fit the FLM (see *Methods* section) for the 10 climate regions. Our aim is to find the possible relationship between the odds of having at least one CDHW-day in a month and the combined effect of large-scale modes of climate variability and ANT based on the observational record. The odds of having at least one CDHW-day in a month indicate the minimum possible risk associated with the increasing anomalies in these global climate patterns and ANT.

Therefore, monthly binary outcomes (0 and 1) of occurrence, and non-occurrence of CDHW day were used as dependent variables into the FLM (see *Methods*). To account for the anthropogenic component into the FLM, changes in the monthly global mean temperature with respect to the pre-industrial period, 1861–1890 was also added as one of the independent variables. Note that all the independent monthly variables (natural and ANT) were first smoothed by applying a 12-month running mean and then regressed against the monthly time series of the binary variable. Finally, the scaling factors and their 5% and 95% confidence intervals (CI) obtained after fitting the FLM for each of the climate regions are shown in Fig. 3. These scaling factors and their CI suggest the multiplicative increase ( $\beta > 1$ ) or decrease ( $\beta < 1$ ) in the monthly odds of a CDHW day for per unit increase in the large-scale climate indices, and ANT. In addition to that, we consider a signal from these large-scale natural modes of climate variability and ANT to have been detected when the CI do not cross zero and consider only the detected signals in our further discussion.

The results (scaling factor, 5% to 95% CI) from the sensitivity analysis suggest that the rise in ANT has a statistically significant positive impact on the odds of occurrence of CDHW days for all selected climate regions, CEU ( $4.1, 2.9\text{--}5.2$ ), CAN ( $3.8, 2.7\text{--}4.9$ ), EAS ( $5.6, 4.1\text{--}7.3$ ), ENA ( $2.9, 2\text{--}3.9$ ), MED ( $4.2, 3\text{--}5.6$ ), NAU ( $3.7, 2.7\text{--}4.9$ ), NEB ( $2.2, 1.3\text{--}2.3$ ), SAS ( $4.2, 3\text{--}5.4$ ), WAS ( $3.2, 2\text{--}4.4$ ), and WNA ( $3.3, 2.2\text{--}4.5$ ) (Fig. 3). These findings agree with previous studies that report a substantial increase in dry and hot spells in various regions across the globe due to rise

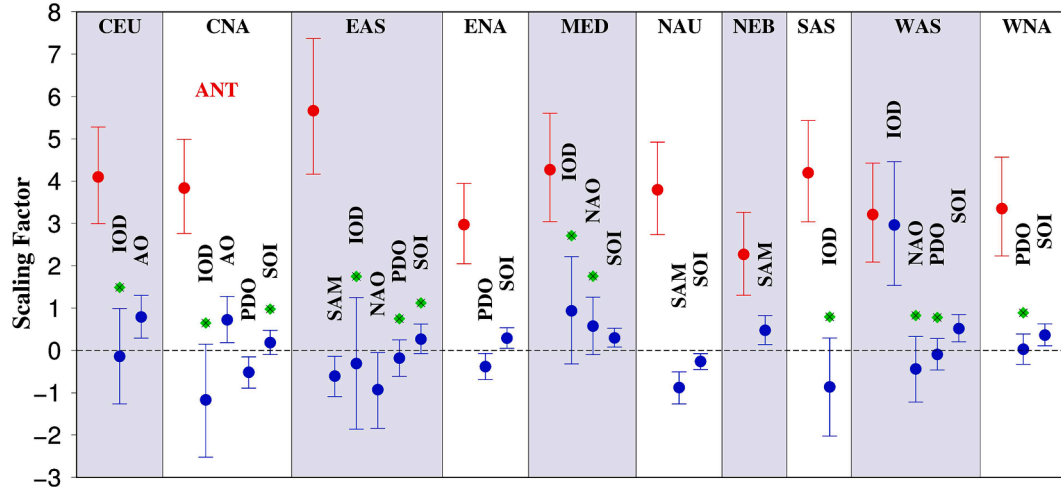


**Fig. 3.** Scaling factors (coefficient of regression) and their corresponding 5–95% CI indicating the sensitivity of odds of occurrence of monthly CDHW days against the inter annual variability of large-scale climate variables and ANT obtained from the FLM for the 10 climate regions. The red color indicates the scaling factors for the ANT, and the blue color indicate the same for the large-scale climate indices. The green circles with a blue cross indicate the scaling factors that are not statistically significant (at 5% significant level). (For interpretation of the references to color in this figure legend, the reader is referred to the web version of this article.)

in global warming (AghaKouchak et al., 2014; Mazdiyasni and AghaKouchak, 2015; Sun et al., 2017, 2018; Zhang et al., 2019). However, depending on the climate regions, the large-scale climate oscillations show either positive or negative signals against the odds of occurrence of CDHW day. For instance, positive phase of SOI shows a statistically significant positive relationship (scaling factor, 5% to 95% CI) for the climate regions, ENA (0.29, 0.05–0.53), MED (0.29, 0.07–0.53), WAS (0.51, 0.11–0.62), and WNA (0.36, 0.11–0.62), while a negative relationship for NAU (−0.25, −0.44 to −0.07). Similarly, significant effect of SAM can be seen for the climate regions, EAS (−0.6, −1.08 to −0.14), NAU (−0.87, −1.26 to −0.5), and NEB (0.47, 0.14–0.82). Increase in positive AO show a significantly positive relationship with the odds of CDHW day for the climate regions, CEU (0.79, 0.29–1.3), CAN (0.72, 0.18–1.2), and increase in positive PDO showed a statistically significant negative relationship for the climate regions, CAN (−0.51, −0.88 to −0.14), and ENA (−0.379, −0.69 to −0.07). On the other hand, NAO and IOD show significantly negative, and positive relationship with the odds of CDHW day for the climate regions, EAS (−0.92, −1.8 to −0.05), and WAS (2.96, 1.53–4.45), respectively. However, for SAS no statistically significant signal is found from the natural variability of the climate.

Thus, CDHW occurrences can be strongly attributable to the ANT, while natural variability has a very weak or no significant (in case of SAS) influence over the odds of CDHW events for the selected regions. Furthermore, the overall relationship of the natural modes of climate variability and ANT with the odds of occurrence of CDHW day (Fig. 3) are found to be consistent with that obtained from the correlation analysis with the MT-CDHW events (Fig. 2a) over the same climate regions.

### 3.5. Effect of 1.5 °C and 2 °C rise in global warming

From the sensitivity analysis, the monthly odds of occurrence of observed CDHW days can be attributed to the rise in ANT in almost all of the climate regions. Moreover, the magnitude of the scaling factors for all the climate regions indicates a substantial increase in the odds with per unit rise in the ANT forcing in the future climate. Given the continuous rise in global temperatures, it is likely that global warming may exceed the 1.5 °C and 2 °C warming levels by the 2030, and mid-21st century, respectively (Lee et al., 2021), which indicates a possibility of higher odds in the future compared to the present climate. To see the likely level of increase, we estimated the ORs for these climate regions as the ratio of monthly odds of occurrence of CDHW day in the 1.5 °C, and 2 °C warming levels to that in the current warming level.

Fig. 4 presents the two-dimensional CI plot showing the OR and the

corresponding CI for the studied regions that show significant DSHW towards drought based on the observational record (Fig. 1d). We find OR (5–95% CI) as high as 3.5 (2.5–5.2), 2.6 (1.98–3.5), 2.5 (1.9–3.4), 2.5 (1.9–3.2), 2.4 (1.8–3), 2.3 (1.8–3), 2.1 (1.6–2.8), 2 (1.6–2.7), 1.9 (1.6–2.4), and 1.7 (1.3–2) for the climate regions, EAS, MED, SAS, CEU, CAN, NAU, WNA, WAS, ENA, and NEB, respectively (Fig. 4). These results suggest greater than 1.7-fold increase in the odds of CDHW is likely in the 1.5 °C warmer world compared to the present climate. Note that EAS exhibit even higher (3.5-fold) increase.

On the other hand, at the 2 °C warming level, EAS, MED, SAS, CEU, CNA, NAU, WNA, WAS, ENA, and NEB, are likely to show ORs of 60.8 (20.4–209.18), 22.1 (9.1–58), 20.9 (9–51.3), 19.5 (8.7–45.9), 16.1 (7.4–37.2), 15.7 (7.2–35.5), 11.36 (5–27.4), 10.26 (4.5–24.7), 8.6 (4.4–17.5), and 5.2 (2.6–10.7), respectively (Fig. 4). Therefore, climate regions such as, MED, and SAS show about 20-fold increase; CEU, CNA, and NAU show more than 15-fold increase; WNA, and WAS show more than 10-fold increase, and ENA, and NEB show 5–8-fold increase in the 2 °C warmer world. Again, EAS shows exceptionally higher levels of odds of having CDHW day in a month with a 60-fold increase at 2 °C warming. Therefore, limiting global warming to 1.5 °C level can substantially limit the risk of increase in the odds of CDHW day in a month, as it can mitigate more than 17-fold increase over EAS, 5–8-fold increase over WNA, NAU, CAN, CEU, SAS, and MED, and 3–4-fold increase over NEB, ENA, WAS when compared to the odds at 2 °C warming level. These results suggest pursuing active efforts to keep the warming levels well below the 2 °C limit (Rogelj et al., 2016).

### 4. Summary and conclusion

Precipitation and temperature variability is affected by the large-scale climate perturbations that often lead to the formation of anticyclonic weather regimes. Under such circumstances, the net radiation received during the daytime becomes the primary component in the surface energy budget that heats up the land surface (Betts et al., 1996). The heating process has been accelerated and further intensified by the increased emission of heat trapping gases due to anthropogenic activities (Samset, 2018) and conditions favored by large scale teleconnections (Mukherjee et al., 2020), leading to increased probability of co-occurrence of HW, and drought events. This study provides a quantitative assessment of the relative effect of anthropogenic warming and large-scale teleconnection patterns on the occurrence of CDHW events during the instrumental period, 1982–2016.

In this study, observational evidence has been provided that suggest a substantial increase in the number of CDHW events per year (1–5 events per year) across various parts of the globe in the beginning of 21st

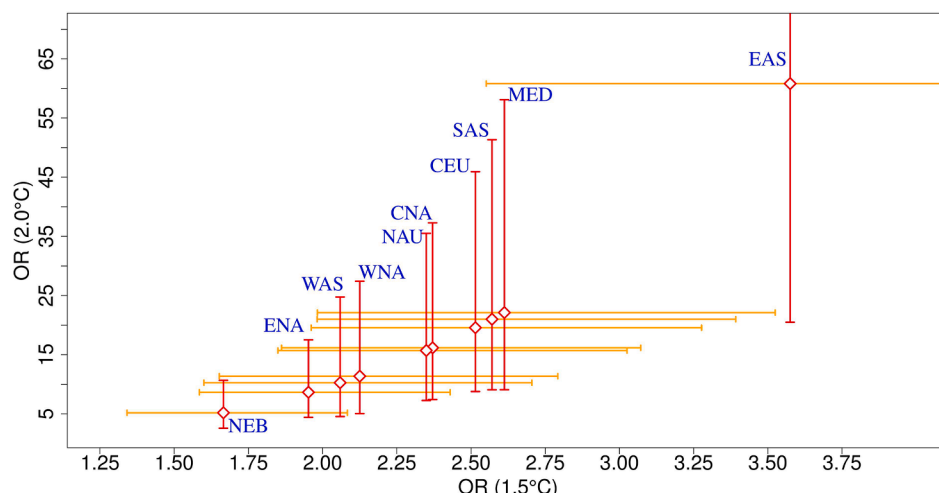


Fig. 4. Ratio of odds (OR) for 1.5 °C and 2 °C warming limits with respect to the current level of warming.

century (2000–2016). HW events were found to be susceptible to the existing drought conditions to different levels in the different global climate regions. For example, out of all the 26 climate regions, only fifteen showed a significant DSHW to the existing drought conditions over more than 2/3rd of their corresponding total area. Out of these 15 regions, the top 10 climate regions, showing the greatest magnitudes of DSHW, are selected for the subsequent analyses. Monthly total number of CDHW days showed significant positive and negative correlation with the interannual variability of few natural modes of climate variability in some of these climate regions. In contrast, anthropogenic warming showed significant positive correlation over all the climate regions during the observational period (1982–2016). Keeping in mind the various shortcomings of the correlation coefficients, such as the susceptibility to outliers and errors arising from linearization, we selected the potential large-scale climate indices based on the literature review to avoid any statistical artifact in the results. Attribution study performed based on a logistic regression approach suggest a significantly positive, and multiplicative effect of anthropogenic global warming on the odds of CDHW occurrences in the most vulnerable climate regions. Finally, odd ratios were estimated for these climate regions that were found to be in the range of 1.7–3.5, and as high as 5–60 at 1.5 °C, and 2 °C warming levels, respectively, with respect to the current world. Moreover, these odd ratios suggest about 17-fold reduction in the odds over EAS, 5–8-fold reduction over WNA, NAU, CAN, CEU, SAS, and MED, and 3–4-fold reduction over NEB, ENA, WAS at the 1.5 °C global warming level, compared to the 2 °C global warming level. Our findings show that among all the climate regions, EAS is the most affected region due to the rise in anthropogenic warming.

Overall, this study offers a quantitative assessment and understanding of the combined effects of natural climate variability and anthropogenic warming on the CDHW events during the past few decades. Nevertheless, future period may see more amplified large-scale teleconnections that may balance or reinforce the impact from increasing anthropogenic warming. Therefore, further scope of improvements in such projections can be accomplished by incorporating the possible effect of warming on large-scale climate perturbations. Even anticyclonic weather regimes, which are accompanied by slow-moving jet or stationary blocking zones (caused by the relatively high-pressure ridges), may also get affected by increase in warming levels (Dong et al., 2018), therefore, should also be considered as additional co-factors. Besides that, a detailed analysis including the multiple components of human influences, such as the land-use practices (Findell et al., 2017), increased effect of dust aerosol (Huang et al., 2015), and surface-energy partitioning (Mukherjee and Mishra, 2020) can also be beneficial for accurately assessing the future changes in CDHW event characteristics. Lastly, simple regression techniques can only identify the relationships between variables and the CDHW events. These techniques are restricted by model assumptions and have limitations in terms of defining the causal linkages that often are more meaningful for prediction purposes, therefore, necessitating development of more nuanced statistical techniques that robustly captures the causal associations between the drivers and CDHW events.

#### CRediT authorship contribution statement

**Sourav Mukherjee:** Conceptualization, Data curation, Formal analysis, Investigation, Methodology, Visualization, Validation, Writing-original draft. **Ashok Mishra:** Conceptualization, Methodology, Project Administration, Resources, Supervision, Writing-review & editing. **Moetasim Ashfaq:** Conceptualization, Methodology, Supervision, Writing-review & editing. **Shih-Chieh Kao:** Conceptualization, Methodology, Writing-review & editing

#### Declaration of Competing Interest

The authors declare that they have no known competing financial

interests or personal relationships that could have appeared to influence the work reported in this paper.

#### Acknowledgments

This study was supported by the National Science Foundation (NSF) award # 1653841 in collaboration with the National Climate-Computing Research Center, which is located within the National Center for Computational Sciences at the ORNL and supported under a Strategic Partnership Project, 2316-T849-08, between DOE and NOAA. We are thankful for the data provided by the NOAA/OAR/ESRL PSD, Boulder, Colorado, USA, from their website at <https://psl.noaa.gov/data/gredded/data.cpc.globaltemp.html>, Global Precipitation Climatology Center (GPCC; <https://www.dwd.de/EN/ourservices/gpcc/gpcc.html>), HadCRUT4 (from <https://crudata.uea.ac.uk/cru/data/temperature/>), and Coupled Model Intercomparison Project Phase-5 (CMIP5; <https://esgf-node.llnl.gov/search/cmip5/>).

#### Appendix A. Supplementary data

Supplementary data to this article can be found online at <https://doi.org/10.1016/j.jhydrol.2021.127396>.

#### References

Abid, M.A., Ashfaq, M., Kucharski, F., Evans, K.J., Almazroui, M., 2020. Tropical Indian ocean mediates ENSO influence over central Southwest Asia during the wet season. *e2020GL089308* Geophys. Res. Lett. 47. <https://doi.org/10.1029/2020GL089308>.

AghaKouchak, A., Cheng, L., Mazdiyasni, O., Farahmand, A., 2014. Global warming and changes in risk of concurrent climate extremes: insights from the 2014 California drought. *Geophys. Res. Lett.* 41 (24), 8847–8852. <https://doi.org/10.1002/2014GL062308>.

Albert, A., Anderson, J.A., 1984. On the existence of maximum likelihood estimates in logistic regression models. *Biometrika* 71, 1–10. <https://doi.org/10.2307/2336390>.

Allen, C.D., Macalady, A.K., Chenchoune, H., Bachelet, D., McDowell, N., Vennetier, M., Kitzberger, T., Rigling, A., Breshears, D.D., Hogg, E.H., Gonzalez, P., Fensham, R., Zhang, Z., Castro, J., Demidova, N., Lim, J.-H., Allard, G., Running, S.W., Semerci, A., Cobb, N., 2010. A global overview of drought and heat-induced tree mortality reveals emerging climate change risks for forests. *For. Ecol. Manag.* Adaptat. For. For. Manage. Chang. Clim. 259 (4), 660–684. <https://doi.org/10.1016/j.foreco.2009.09.001>.

Ashok, K., Saji, N.H., 2007. On the impacts of ENSO and Indian Ocean dipole events on sub-regional Indian summer monsoon rainfall. *Nat. Hazards* 42 (2), 273–285.

Barlow, M., Cullen, H., Lyon, B., 2002. Drought in central and Southwest Asia: La Niña, the warm pool, and indian ocean precipitation. *J. Clim.* 15, 697–700. [https://doi.org/10.1175/1520-0442\(2002\)015<0697:DICASA>2.0.CO;2](https://doi.org/10.1175/1520-0442(2002)015<0697:DICASA>2.0.CO;2).

Betts, A.K., Ball, J.H., Beljaars, A.C.M., Miller, M.J., Viterbo, P.A., 1996. The land surface-atmosphere interaction: a review based on observational and global modeling perspectives. *J. Geophys. Res. Atmos.* 101 (D3), 7209–7225. <https://doi.org/10.1029/95JD02135>.

Ballasina, M.A., Messori, G., 2018. On the link between the subseasonal evolution of the North Atlantic Oscillation and East Asian climate. *Clim. Dyn.* 51 (9–10), 3537–3557. <https://doi.org/10.1007/s00382-018-4095-5>.

Cassou, C., Terray, L., Phillips, A.S., 2005. Tropical atlantic influence on European heat waves. *J. Clim.* 18, 2805–2811. <https://doi.org/10.1175/JCLI3506.1>.

Cias, P.H., Reichstein, M., Viovy, N., Granier, A., Ogée, J., Allard, V., Aubinet, M., Buchmann, N., Bernhofer, C., Carrara, A., Chevallier, F., De Noblet, N., Friend, A.D., Friedlingstein, P., Grünwald, T., Heinrichs, B., Kerone, P., Knobh, A., Krinner, G., Loustau, D., Manca, G., Matteucci, G., Miglietta, F., Ourcival, J.M., Papale, D., Pilegaard, K., Rambal, S., Seufert, G., Soussana, J.F., Sanz, M.J., Schulze, E.D., Vesala, T., Valentini, R., 2005. Europe-wide reduction in primary productivity caused by the heat and drought in 2003. *Nature* 437 (7058), 529–533. <https://doi.org/10.1038/nature03972>.

Dai, A., Zhao, T., 2017. Uncertainties in historical changes and future projections of drought: Part I: estimates of historical drought changes. *Clim. Change* 144 (3), 519–533. <https://doi.org/10.1007/s10584-016-1705-2>.

Deng, K., Yang, S., Ting, M., Lin, A., Wang, Z., 2018. An intensified mode of variability modulating the summer heat waves in eastern Europe and northern China. *Geophys. Res. Lett.* 45, 11–361.

Dong, L., Mitra, C., Greer, S., Burt, E., Dong, L., Mitra, C., Greer, S., Burt, E., 2018. The dynamical linkage of atmospheric blocking to drought, heatwave and urban heat island in southeastern US: a multi-scale case study. *Atmosphere* 9, 33. <https://doi.org/10.3390/atmos9010033>.

Dulière, V., Zhang, Y., Salathé, E.P., 2013. Changes in twentieth-century extreme temperature and precipitation over the western united states based on observations and regional climate model simulations. *J. Clim.* 26, 8556–8575. <https://doi.org/10.1175/JCLI-D-12-00818.1>.

Filippi, L., Palazzi, E., von Hardenberg, J., Provenzale, A., 2014. Multidecadal Variations in the Relationship between the NAO and Winter Precipitation in the Hindu Kush-Karakoram. *J. Clim.* 27, 7890–7902. <https://doi.org/10.1175/JCLI-D-14-00286.1>.

Findell, K.L., Berg, A., Gentile, P., Krasting, J.P., Lintner, B.R., Malyshov, S., Santanello, J.A., Shevliakova, E., 2017. The impact of anthropogenic land use and land cover change on regional climate extremes. *Nat. Commun.* 8, 989. <https://doi.org/10.1038/s41467-017-01038-w>.

Fischer, E.M., Knutti, R., 2015. Anthropogenic contribution to global occurrence of heavy-precipitation and high-temperature extremes. *Nat. Clim. Change* 5, 560–564. <https://doi.org/10.1038/nclimate2617>.

Fischer, E.M., Schär, C., 2010. Consistent geographical patterns of changes in high-impact European heatwaves. *Nat. Geosci.* 3 (6), 398–403. <https://doi.org/10.1038/geo866>.

García-Serrano, J., Cassou, C., Douville, H., Giannini, A., Doblas-Reyes, F.J., 2017. Revisiting the ENSO teleconnection to the tropical North Atlantic. *J. Clim.* 30 (17), 6945–6957. <https://doi.org/10.1175/JCLI-D-16-0641.110.1175/JCLI-D-16-0641.1>.

Gillet, N.P., Kell, T.D., Jones, P.D., 2006. Regional climate impacts of the Southern Annular Mode. *Geophys. Res. Lett.* 33 (23) <https://doi.org/10.1029/2006GL027721>.

Guan, Z., Yamagata, T., 2003. The unusual summer of 1994 in East Asia: IOD teleconnections. *Geophys. Res. Lett.* 30 (10), n/a–n/a. <https://doi.org/10.1029/2002GL016831>.

Hao, Z., Hao, F., Singh, V.P., Zhang, X., 2019. Statistical prediction of the severity of compound dry-hot events based on El Niño-Southern Oscillation. *J. Hydrol.* 572, 243–250. <https://doi.org/10.1016/j.jhydrol.2019.03.001>.

Hao, Z., Hao, F., Singh, V.P., Zhang, X., 2018. Quantifying the relationship between compound dry and hot events and El Niño-southern Oscillation (ENSO) at the global scale. *J. Hydrol.* 567, 332–338. <https://doi.org/10.1016/j.jhydrol.2018.10.022>.

Hassan, W.U., Nayak, M.A., 2020. Global teleconnections in droughts caused by oceanic and atmospheric circulation patterns. *Environ. Res. Lett.* 16 (1), 014007. <https://doi.org/10.1088/1748-9326/abc9e2>.

Horton, R.M., Mankin, J.S., Lesk, C., Coffel, E., Raymond, C., 2016. A review of recent advances in research on extreme heat events. *Curr. Clim. Change Rep.* 2 (4), 242–259. <https://doi.org/10.1007/s40641-016-0042-x>.

Hu, Z.-Z., Huang, B., 2009. Interferential impact of ENSO and PDO on dry and wet conditions in the US Great Plains. *J. Clim.* 22, 6047–6065.

Huang, J.P., Liu, J.J., Chen, B., Nasiri, S.L., 2015. Detection of anthropogenic dust using CALIPSO lidar measurements. *Atmos. Chem. Phys.* 15, 11653–11665. <https://doi.org/10.5194/acp-15-11653-2015>.

Knight, J.R., Folland, C.K., Scaife, A.A., 2006. Climate impacts of the atlantic multidecadal oscillation. *Geophys. Res. Lett.* 33 (17) <https://doi.org/10.1029/2006GL026242>.

Lau, W.K.M., Kim, K.-M., 2012. The 2010 pakistan flood and russian heat wave: teleconnection of hydrometeorological extremes. *J. Hydrometeorol.* 13, 392–403. <https://doi.org/10.1175/JHM-D-11-0161>.

Lee, J.-Y., Marotzke, G., Bala, L., Cao, S., Corti, J.P., Dunne, F., Engelbrecht, E., Fischer, J., C. Fyfe, C., Jones, A., Maycock, J., Mutemi, O., Ndiaye, S., Panickal, and T. Zhou: 2021, Future Global Climate: Scenario-Based Projections and Near-Term Information. In: Climate Change 2021. In Masson-Delmotte, V., P. Zhai, A. Pirani, S.L. Connors, C. Péan, S. Berger, N. Caud, Y. Chen, L. Goldfarb, M.I. Gomis, M. Huang, K. Leitzell, E. Lonnoy, J.B.R. Matthews, T.K. Maycock, T. Waterfield, O. Yelekçi, R. Yu, and B. Zhou (Eds.), The Physical Science Basis. Contribution of Working Group I to the Sixth Assessment Report of the Intergovernmental Panel on Climate Change. Cambridge University Press. In Press.

Lindsey, J.K., 2000. *Applying Generalized Linear Models*. Springer Science & Business Media.

Lu, J., Vecchi, G.A., Reichler, T., 2007. Expansion of the Hadley cell under global warming. *Geophys. Res. Lett.* 34 (6) <https://doi.org/10.1029/2006GL028443>.

Mahlstein, I., Martius, O., Chevalier, C., Ginsbourger, D., 2012. Changes in the odds of extreme events in the Atlantic basin depending on the position of the extratropical jet. *Geophys. Res. Lett.* 39 (22), n/a–n/a. <https://doi.org/10.1029/2012GL053993>.

Manatsa, D., Chingombe, W., Matararia, C.H., 2008. The impact of the positive Indian ocean dipole on zimbabwe droughts. *Int. J. Climatol. J. R. Meteorol. Soc.* 28 (15), 2011–2029.

Marshall, A.G., Hudson, D., Wheeler, M.C., Alves, O., Hendon, H.H., Pook, M.J., Risbey, J.S., 2014. Intra-seasonal drivers of extreme heat over Australia in observations and POAMA-2. *Clim. Dyn.* 43 (7–8), 1915–1937. <https://doi.org/10.1007/s00382-013-2016-1>.

Mazdiyasni, O., AghaKouchak, A., 2015. Substantial increase in concurrent droughts and heatwaves in the United States. *Proc. Natl. Acad. Sci. U.S.A.* 112 (37), 11484–11489. <https://doi.org/10.1073/pnas.1422945112>.

McCabe, G.J., Palecki, M.A., Betancourt, J.L., 2004. Pacific and Atlantic Ocean influences on multidecadal drought frequency in the United States. *Proc. Natl. Acad. Sci. U.S.A.* 101 (12), 4136–4141. <https://doi.org/10.1073/pnas.0306738101>.

Meehl, G.A., Tebaldi, C., 2004. More intense, more frequent, and longer lasting heat waves in the 21st century. *Science* 305 (5686), 994–997.

Meyers, G., McIntosh, P., Pigot, L., Pook, M., 2007. The Years of El Niño, La Niña, and Interactions with the Tropical Indian Ocean. *J. Clim.* 20, 2872–2880. <https://doi.org/10.1175/JCLI4152.1>.

Morice, C.P., Kennedy, J.J., Rayner, N.A., Jones, P.D., 2012. Quantifying uncertainties in global and regional temperature change using an ensemble of observational estimates: The HadCRUT4 data set. *J. Geophys. Res. Atmos.* 117 (D8), n/a–n/a. <https://doi.org/10.1029/2011JD017187>.

Mukherjee, S., Ashfaq, M., Mishra, A.K., 2020. Compound drought and heatwaves at a global scale: the role of natural climate variability-associated synoptic patterns and land-surface energy budget anomalies. *J. Geophys. Res. Atmos.* 125 e2019JD031943.

Mukherjee, S., Mishra, A., Trenberth, K.E., 2018. Climate change and drought: a perspective on drought indices. *Curr. Clim. Change Rep.* 4 (2), 145–163. <https://doi.org/10.1007/s40641-018-0098-x>.

Mukherjee, S., Mishra, A.K., 2020. Increase in compound drought and heatwaves in a warming world. *e2020GL090617 Geophys. Res. Lett.* <https://doi.org/10.1029/2020GL090617>.

Pepler, A., Dowdy, A., Hope, P., 2019. A global climatology of surface anticyclones, their variability, associated drivers and long-term trends. *Clim. Dyn.* 52 (9–10), 5397–5412. <https://doi.org/10.1007/s00382-018-4451-5>.

Perkins, S.E., Alexander, L.V., Nairn, J.R., 2012. Increasing frequency, intensity and duration of observed global heatwaves and warm spells. *Geophys. Res. Lett.* 39 (20) <https://doi.org/10.1029/2012GL053361>.

Perkins, S.E., Argüeso, D., White, C.J., 2015. Relationships between climate variability, soil moisture, and Australian heatwaves. *J. Geophys. Res. Atmos.* 120 (16), 8144–8164. <https://doi.org/10.1002/2015JD023592>.

Peterson, T.C., Heim, R.R., Hirsch, R., Kaiser, D.P., Brooks, H., Diffenbaugh, N.S., Dole, R.M., Giovannettone, J.P., Guirguis, K., Karl, T.R., Katz, R.W., Kunkel, K., Lettermaier, D., McCabe, G.J., Paciorek, C.J., Ryberg, K.R., Schubert, S., Silva, V.B., Stewart, B.C., Vecchia, A.V., Villarini, G., Vose, R.S., Walsh, J., Wehner, M., Wolock, D., Wolter, K., Woodhouse, C.A., Wuebbles, D., 2013. Monitoring and understanding changes in heat waves, cold waves, floods, and droughts in the United States: state of knowledge. *Bull. Am. Meteorol. Soc.* 94 (6), 821–834. <https://doi.org/10.1175/BAMS-D-12-00066.1>.

Poumadière, M., Mays, C., Le Mer, S., Blong, R., 2005. The 2003 heat wave in France: dangerous climate change here and now. *Risk Anal. Off. Publ. Soc. Risk Anal.* 25, 1483–1494. <https://doi.org/10.1111/j.1539-6924.2005.00694.x>.

Qiu, Y., Cai, W., Guo, X., Ng, B., 2014. The asymmetric influence of the positive and negative IOD events on China's rainfall. *Sci. Rep.* 4, 4943. <https://doi.org/10.1038/srep04943>.

Rajagopalan, B., Cook, E., Lall, U., Ray, B.K., 2000. Spatiotemporal variability of ENSO and SST teleconnections to summer drought over the united states during the twentieth century. *J. Clim.* 13, 4244–4255. [https://doi.org/10.1175/1520-0442\(2000\)013<4244:SVOEAS>2.0.CO;2](https://doi.org/10.1175/1520-0442(2000)013<4244:SVOEAS>2.0.CO;2).

Rogelj, J., den Elzen, M., Höhne, N., Fransen, T., Fekete, H., Winkler, H., Schaeffer, R., Sha, F., Riahi, K., Meinshausen, M., 2016. Paris agreement climate proposals need a boost to keep warming well below 2 °C. *Nature* 534, 631–639. <https://doi.org/10.1038/nature18307>.

Roxy, M.K., Ritika, K., Terray, P., Murtugudde, R., Ashok, K., Goswami, B.N., 2015. Drying of Indian subcontinent by rapid Indian Ocean warming and a weakening land-sea thermal gradient. *Nat. Commun.* 6, 7423. <https://doi.org/10.1038/ncomms8423>.

Saji, N.H., Yamagata, T., 2003. Possible impacts of Indian Ocean Dipole mode events on global climate. *Clim. Res.* 25, 151–169. <https://doi.org/10.3384/cr025151>.

Samset, B.H., 2018. How cleaner air changes the climate. *Science* 360 (6385), 148–150.

Sanford, T., Frumhoff, P.C., Luers, A., Guldledge, J., 2014. The climate policy narrative for a dangerously warming world. *Nat. Clim. Change* 4 (3), 164–166. <https://doi.org/10.1038/nclimate2148>.

Schamm, K., Ziese, M., Raykova, K., Becker, A., Finger, P., Meyer-Christoffer, A., Schneider, U., 2015. GPCC full data daily version 1.0 at 1.0: Daily land-surface precipitation from rain-gauges built on GTS-based and historic data. DOI.

Seneviratne, S.I., Corti, T., Davin, E.L., Hirschi, M., Jaeger, E.B., Lehner, I., Orlowsky, B., Teuling, A.J., 2010. Investigating soil moisture–climate interactions in a changing climate: a review. *Earth-Sci. Rev.* 99 (3–4), 125–161. <https://doi.org/10.1016/j.earscirev.2010.02.004>.

Singh, J., Ashfaq, M., Skinner, C.B., Anderson, W.B., Singh, D., 2021. Amplified risk of spatially compounding droughts during co-occurrences of modes of natural ocean variability. *NPJ Clim. Atmos. Sci.* 4, 1–14. <https://doi.org/10.1038/s41612-021-00161-2>.

Song, F., Zhou, T., 2013. Interannual variability of east asian summer monsoon simulated by CMIP3 and CMIP5 AGCMs: skill dependence on indian ocean-western pacific anticyclone teleconnection. *J. Clim.* 27, 1679–1697. <https://doi.org/10.1175/JCLI-D-13-00248.1>.

Stefanou, M., Drobinski, P., D'Andrea, F., Lebeaupin-Brossier, C., Bastin, S., 2014. Soil moisture-temperature feedbacks at meso-scale during summer heat waves over Western Europe. *Clim. Dyn.* 42 (5–6), 1309–1324. <https://doi.org/10.1007/s00382-013-1794-9>.

Sun, Q., Miao, C., AghaKouchak, A., Duan, Q., 2017. Unraveling anthropogenic influence on the changing risk of heat waves in China. *Geophys. Res. Lett.* 44 (10), 5078–5085. <https://doi.org/10.1029/2017GL073531>.

Sun, Z., Ouyang, Z., Zhao, J., Li, S., Zhang, X., Ren, W., 2018. Recent rebound in observational large-pan evaporation driven by heat wave and droughts by the Lower Yellow River. *J. Hydrol.* 565, 237–247. <https://doi.org/10.1016/j.jhydrol.2018.08.014>.

Trenberth, K.E., Dai, A., van der Schrier, G., Jones, P.D., Barichivich, J., Briffa, K.R., Sheffield, J., 2014. Global warming and changes in drought. *Nat. Clim. Change* 4 (1), 17–22. <https://doi.org/10.1038/nclimate2067>.

Trenberth, K.E., Faloutsos, J.T., 2012. Climate extremes and climate change: the Russian heat wave and other climate extremes of 2010. *J. Geophys. Res. Atmos.* 117 (D17), n/a–n/a. <https://doi.org/10.1029/2012JD018020>.

Trouet, V., Babst, F., Meko, M., 2018. Recent enhanced high-summer North Atlantic Jet variability emerges from three-century context. *Nat. Commun.* 9, 180. <https://doi.org/10.1038/s41467-017-02699-3>.

Unkašević, M., Tošić, I., 2013. Trends in temperature indices over Serbia: Relationships to large-scale circulation patterns. *Int. J. Climatol.* 33 (15), 3152–3161. <https://doi.org/10.1002/joc.3652>.

Wang, B., Zhang, Q., 2002. Pacific-east asian teleconnection. Part II: how the philippine sea anomalous anticyclone is established during El Niño development. *J. Clim.* 15, 3252–3265. [https://doi.org/10.1175/1520-0442\(2002\)015<3252:PEATPI>2.0.CO;2](https://doi.org/10.1175/1520-0442(2002)015<3252:PEATPI>2.0.CO;2).

Wang, C., Deser, C., Yu, J.-Y., DiNezio, P., Clement, A., 2017. El Niño and southern oscillation (ENSO): a review. In: Glynn, P.W., Manzello, D.P., Enochs, I.C. (Eds.), *Coral Reefs of the Eastern Tropical Pacific: Persistence and Loss in a Dynamic Environment, Coral Reefs of the World*. Springer, Dordrecht, pp. 85–106. [https://doi.org/10.1007/978-94-017-7499-4\\_4](https://doi.org/10.1007/978-94-017-7499-4_4).

Wang, L., Yuan, X., Xie, Z., Wu, P., Li, Y., 2016. Increasing flash droughts over China during the recent global warming hiatus. *Sci. Rep.* 6, 30571. <https://doi.org/10.1038/srep30571>.

Webb, R., Rosenzweig, C.E., Levine, E.R., 2000. Global Soil Texture and Derived Water-Holding Capacities (Webb et al.). ORNL DAAC. <https://doi.org/10.3334/ORNLDaac/548>.

Wells, N., Goddard, S., Hayes, M.J., 2004. A self-calibrating palmer drought severity index. *J. Clim.* 17, 2335–2351. [https://doi.org/10.1175/1520-0442\(2004\)017<2335:ASPDSE>2.0.CO;2](https://doi.org/10.1175/1520-0442(2004)017<2335:ASPDSE>2.0.CO;2).

Whan, K., Zscheischler, J., Orth, R., Shongwe, M., Rahimi, M., Asare, E.O., Seneviratne, S.I., 2015. Impact of soil moisture on extreme maximum temperatures in Europe. *Weather Clim. Extrem.*, The World Climate Research Program Grand Challenge on Extremes – WCRP-ICTP Summer School on Attribution and Prediction of Extreme Events 9, 57–67. <https://doi.org/10.1016/j.wace.2015.05.001>.

Wu, Z., Dou, J., Lin, H., 2015. Potential influence of the November–December Southern Hemisphere annular mode on the East Asian winter precipitation: a new mechanism. *Clim. Dyn.* 44 (5–6), 1215–1226. <https://doi.org/10.1007/s00382-014-2241-2>.

Yin, J.H., 2005. A consistent poleward shift of the storm tracks in simulations of 21st century climate. *Geophys. Res. Lett.* 32 (18), n/a–n/a. <https://doi.org/10.1029/2005GL023684>.

Yu, E., King, M.P., Sobolowski, S., Otterå, O.H., Gao, Y., 2018. Asian droughts in the last millennium: a search for robust impacts of Pacific Ocean surface temperature variabilities. *Clim. Dyn.* 50 (11–12), 4671–4689. <https://doi.org/10.1007/s00382-017-3897-1>.

Zampieri, M., Ceglar, A., Dentener, F., Toreti, A., 2017. Wheat yield loss attributable to heat waves, drought and water excess at the global, national and subnational scales. *Environ. Res. Lett.* 12 (6), 064008. <https://doi.org/10.1088/1748-9326/aa723b>.

Zhai, P., Zhang, X., Wan, H., Pan, X., 2005. Trends in total precipitation and frequency of daily precipitation extremes over China. *J. Clim.* 18, 1096–1108. <https://doi.org/10.1175/JCLI-3318.1>.

Zhang, W., Wang, Z., Stuecker, M.F., Turner, A.G., Jin, F.-F., Geng, X., 2019a. Impact of ENSO longitudinal position on teleconnections to the NAO. *Clim. Dyn.* 52 (1–2), 257–274. <https://doi.org/10.1007/s00382-018-4135-1>.

Zhang, Y., You, Q., Mao, G., Chen, C., Ye, Z., 2019b. Short-term concurrent drought and heatwave frequency with 1.5 and 2.0 °C global warming in humid subtropical basins: a case study in the Gan River Basin, China. *Clim. Dyn.* 52 (7–8), 4621–4641. <https://doi.org/10.1007/s00382-018-4398-6>.